Characterization of sensing capability of optofluidic ring resonator biosensors

Hao Li[1,2] and Xudong Fan[1,a)]
[1]*Department of Biomedical Engineering, University of Michigan, 1101 Beal Avenue, Ann Arbor, Michigan 48109, USA*
[2]*Department of Optical Science and Engineering, Key Laboratory for Micro and Nano Photonic Structures (Ministry of Education), Fudan University, Shanghai 200433, People's Republic of China*

(Received 13 May 2010; accepted 17 June 2010; published online 9 July 2010)

The sensing capability of the capillary-based optofluidic ring resonator in bulk refractive index (RI) detection and label-free small molecule detection is investigated. In bulk RI detection, a sensitivity of 570 nm/refractive index units (RIU) is achieved with a Q-factor of 1.2×10^5. A change of 2.8×10^{-7} RIU is observed with the noise equivalent detection limit (NEDL) of 3.8×10^{-8} RIU. In small molecule detection, 10 nM biotin is detected with surface mass density of 1.6 $\mathrm{pg/mm^2}$. The NEDL is approximately 0.14 $\mathrm{pg/mm^2}$. These results set the benchmark for ring resonator sensing performance and compare very favorably with those obtained with other label-free optical sensors. © *2010 American Institute of Physics*. [doi:10.1063/1.3462296]

Optical ring resonators have recently been under intensive investigation as a promising label-free biosensing technology.[1] In a ring resonator, the resonant light circulates along the resonator and interacts with the analytes in buffer (or air). Usually there are two types of detections used in biosensing and analytical chemistry, bulk mass [or refractive index (RI)] detection, in which analytes are present homogeneously in buffer, and surface mass (or RI) detection, in which analytes are present at the solid-liquid interface. In the former case, the RI of the whole portion of the resonant mode in buffer changes, whereas in the latter RI change occurs only near the resonator surface. Both types of RI changes lead to a spectral shift in the resonant wavelength, thus generating a sensing signal. The corresponding sensing capability is characterized by the bulk RI detection limit in units of refractive index units (RIU) or surface mass density detection limit in units of picogram per square millimeter.[1] These two parameters are often used to characterize many other types of label-free optical sensors, allowing for direct comparison among different sensing technologies.

To date, detection of various analytes has been demonstrated with ring resonators.[2–7] Theoretical analysis indicates excellent sensing performance of the ring resonator in bulk RI detection and surface mass detection.[8,9] However, nearly all ring resonator sensing studies performed so far use relatively high bulk RI changes or surface mass densities and then extrapolate the data to obtain the corresponding detection limits. What the sensing capability of a ring resonator can actually achieve under more realistic conditions and how well it compares with other label-free sensors, such as surface plasmon resonance, still remain unanswered.

The aim of this paper is to experimentally characterize the ring resonator's sensing capability in bulk RI detection and surface mass detection, thus setting the benchmark for ring resonator sensing performance. In bulk RI detection, a change of 2.8×10^{-7} RIU is observed with the noise equivalent detection limit (NEDL) of 3.8×10^{-8} RIU. In surface mass density detection, biotin is used as a model system for small molecule detection. 10 nM of biotin is detected, corresponding to a surface mass density of 1.6 $\mathrm{pg/mm^2}$. The NEDL is estimated to be 0.14 $\mathrm{pg/mm^2}$. These results represent the best sensing performance achieved with the ring resonator and compare very favorably with those obtained with other types of label-free optical sensors.

The structure of the ring resonator used in this work is the capillary-based optofluidic ring resonator (OFRR), which has an excellent combination of sensitivity and Q-factor and has been extensively studied in the past few years.[3,10–12] The radial distribution of a resonant mode of the OFRR is described, as follows:[12]

$$E_{m,l}(r) = \begin{cases} AJ_m(k_0^{(m,l)}n_{\mathrm{core}}r), & r \le (R-d_{\mathrm{wall}}) \\ BJ_m(k_0^{(m,l)}n_{\mathrm{wall}}r) + CH_m^{(1)}(k_0^{(m,l)}n_{\mathrm{wall}}r), & (R-d_{\mathrm{wall}}) \le r \le R \\ DH_m^{(1)}(k_0^{(m,l)}n_{\mathrm{air}}r), & r \ge R \end{cases}, \quad (1)$$

where J_m and $H_m^{(1)}$ are the mth Bessel function and the mth Hankel function of the first kind, respectively. n_{core}, n_{wall}, and n_{air} represent the refractive indices of the liquid core, the glass wall, and the surrounding medium. R is the outer radius of the OFRR and d_{wall} is the wall thickness. $k_0^{(m,l)}$ is the amplitude of the resonant wave vector in vacuum labeled by the azimuth index m and the radial index l. In our work, $k_0^{(m,l)}$ is numerically determined by a home-made program based on the Mie theory. In Figs. 1(a)–1(c), the electric field distribution of the third order radial resonant mode around 980 nm is plotted for various wall thicknesses. Their respective bulk refractive index sensitivity (BRIS) is also calculated and plotted in Fig. 1(d). It is showed that the fraction of the mode in the liquid core increases while the wall thickness decreases, providing various kinds of resonant modes for different sensing applications. For bulk RI detection, large fraction of the mode in the liquid core is preferred, whereas for surface detection, large electric field at the OFRR inner surface is preferred. When the wall is 2.5 μm thick, most of the mode (Mode 1) is confined within the wall and is insensitive to bulk or surface RI change. When the wall is 1.9 μm thick,

a)Electronic mail: xsfan@umich.edu.

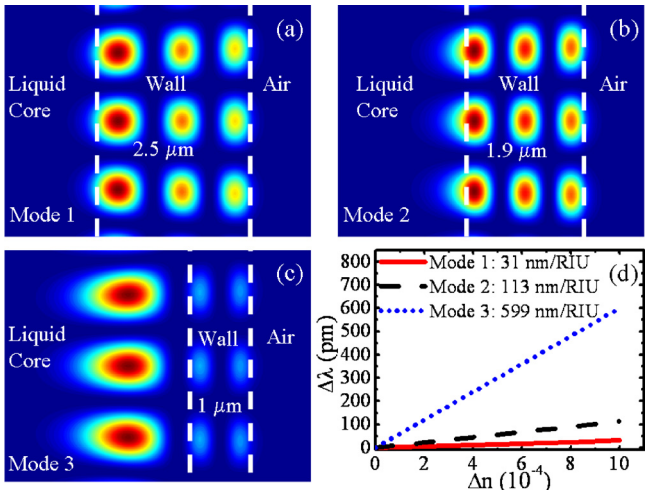

FIG. 1. (Color online) [(a)–(c)] Field distribution of the third order TM-mode around 980 nm obtained using Eq. (1) with different wall thicknesses. (a) d_{wall}=2.5 μm, λ=985.8122 nm, and m=300. (b) d_{wall}=1.9 μm, λ=977.1539 nm, and m=295. (c) d_{wall}=1.0 μm, λ=962.4437 nm, and m=290. In all cases, n_{core}=1.33, n_{wall}=1.45, and n_{air}=1. Outer radius R is 36 μm. (d) The corresponding BRIS.

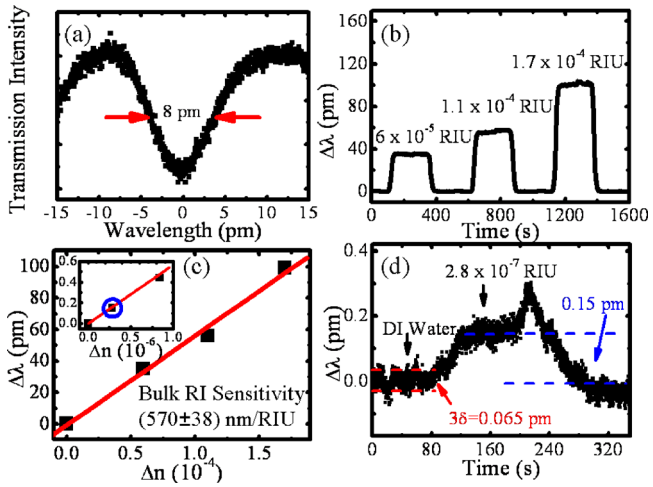

FIG. 3. (Color online) Bulk RI detection. (a) The mode has a Q-factor of 1.2×10^5. (b) Sensorgrams of the OFRR in response to various bulk RI changes in the range of 10^{-5}–10^{-4} RIU. (c) The corresponding BRIS of (570±38) nm/RIU is obtained with linear fitting. The inset shows the response of the same mode to the bulk RI change below 10^{-6} RIU. (d) The sensorgram for detection of 2.8×10^{-7} RIU bulk RI change that corresponds to the data point circled in the inset of (c). The front of the water-ethanol solution arrives at 80 s. The subsequent rinse with DI water occurs at 220 s.

the electric field of Mode 2 peaks near the OFRR inner surface and its sensitivity to surface mass is expected to be high, as suggested by Ref. 9. Further reduction in the wall thickness pushes the mode (Mode 3) well into the liquid core,[11] resulting in extremely high BRIS, which is more applicable for bulk mass detection.

The fabrication of the OFRR is as follows. First, a fused silica tube with an outer diameter (OD) of 0.85 mm and an inner diameter (ID) of 0.7 mm is pre-etched from the outside by hydrofluoric acid (HF), reducing the wall thickness down to about 15 μm. Second, the tube is pulled under CO_2 illumination, as described previously.[12] After pulling, the OD is about 70 μm and the wall thickness is about 2–3 μm. Further chemical etching with diluted HF reduces the wall thickness to about 1 μm for bulk RI detection and 2 μm for surface mass detection.

The experimental setup is illustrated in Fig. 2. The OFRR is placed in an environmentally isolated, thermally controlled copper chamber, and is in contact with a tapered fiber. Light from a 980 nm tunable laser is coupled into the

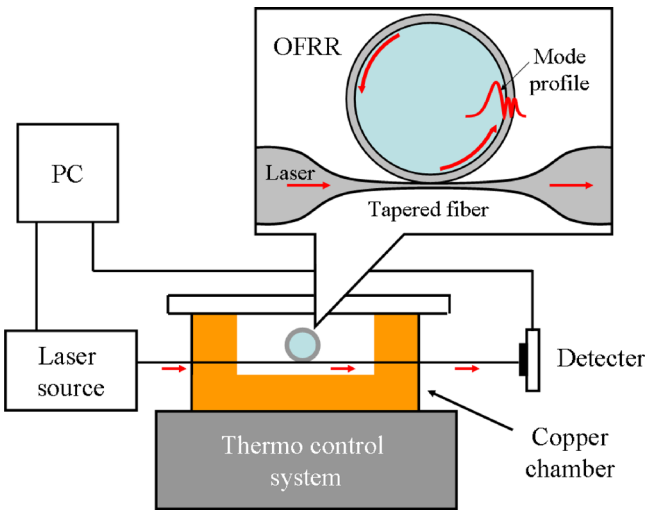

FIG. 2. (Color online) Experiment setup.

OFRR. The laser wavelength is scanned across a range of about 100 pm and the transmission intensity is monitored by a photodetector. The resonant wavelength is determined by Lorentzian-curve fitting the trough in transmission spectrum. The fluids are delivered by a syringe pump at a rate of 100 nL/min.

The results of bulk RI detection are showed in Fig. 3. The resonant mode in Fig. 3(a) has a linewidth of 8 pm, corresponding to a Q-factor of 1.2×10^5, which is limited by the intrinsic water absorption at 980 nm ($Q=4.3\times10^5$) (Ref. 13) and the OFRR surface roughness caused by the chemical etching. The BRIS is measured using various concentrations of ethanol in deionized water (DI water). The sensorgrams corresponding to relatively large RI changes (10^{-5}–10^{-4} RIU) in the core are showed in Fig. 3(b). The linear fit in Fig. 3(c) indicates that this mode has a BRIS of 570 nm/RIU, very close to the simulation result in Fig. 1(c). In order to further test the sensing capability, ethanol solutions with bulk RI changes below 10^{-6} RIU are used. The BRIS shown in the inset of Fig. 3(c) is consistent with that obtained from the higher RI change range. The sensorgram of the lowest RI change, 2.8×10^{-7} RIU, is showed in Fig. 3(d). A 0.15 pm wavelength shift can be clearly distinguished when the ethanol-water mixture replaces DI water initially filled in the OFRR. Subsequent DI water rinse at 220 s brings the mode spectral position back to the baseline, which confirms that the spectral shift is indeed caused by the RI change in the OFRR core. This result demonstrates the bulk RI sensing capability of the ring resonator in the 10^{-7} region. Furthermore, the standard deviation, δ, is obtained to be 0.0217 pm, leading to a bulk RI NEDL of 3.8×10^{-8} RIU, which breaks the barrier of 10^{-7} RIU that label-free biosensors typically encounter.[14]

In surface mass measurement, we choose an OFRR with a wall thickness of about 2 μm. The corresponding BRIS of the mode is approximately 100 nm/RIU and the electric field peaks near the OFRR inner surface, as discussed earlier. The Q-factor of this mode is about 6×10^5. Furthermore, we use

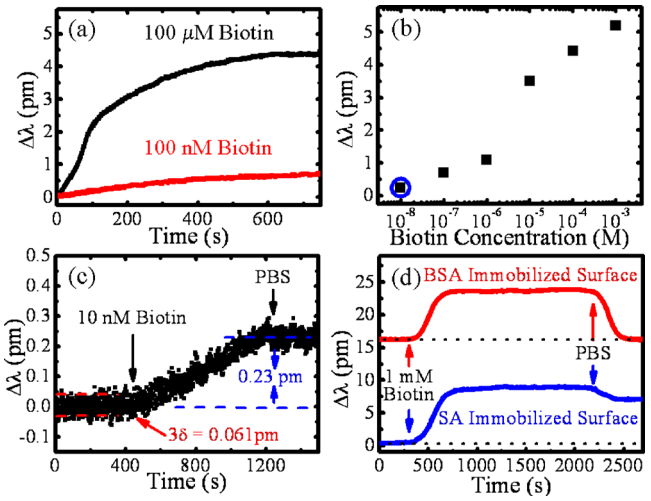

FIG. 4. (Color online) Small molecule detection. (a) Representative sensorgrams for biotin binding to SA immobilized on the OFRR surface. (b) The corresponding spectral shifts obtained 800 s after biotin injection for different biotin concentrations. (c) The sensorgram for detection of 10 nM biotin that corresponds to the data point circled in (b). (d) Upper (lower) curve: negative (positive) control where biotin passes through the OFRR immobilized with BSA (streptavidin). Curves are vertically shifted for clarity.

biotin (molecular weight=244 Da) as a model system to test the small molecule detection capability of the OFRR.[15–19]

To detect biotin, the OFRR inner surface is immobilized with streptavidin (SA) as the capture molecules. First, the OFRR inner surface is silanized with 5% aminopropyltriethoxysilane in water and activated by 2 mM bis(sulfosuccinimidyl) suberate. Then, 0.1 mg/mL SA is flowed for a long time (>1.5 hours). After 0.1 mg/mL BSA blocking, the OFRR is filled with PBS and ready for biotin detection.

The biotin-PBS solution is then pumped through the OFRR. Multiple experiments are carried out for various concentrations of biotin from 10 nM to 1 mM. Two typical binding curves of 100 nM and 100 μM biotin are shown in Fig. 4(a). Figure 4(b) plots the mode spectral shift obtained 800 s after biotin injection for different biotin concentrations. The largest shift is 5.2 pm caused by 1 mM biotin, corresponding to a biotin surface mass density of 36 pg/mm^2 based on the theory described in Ref. 3. The biotin-SA ratio is estimated to be 3.2:1 if the OFRR surface is assumed to be fully covered with SA (i.e., 2.44 ng/mm^2), based on our previous studies.[3] Note that the dissociation constant, K_d, obtained from Fig. 4(b) is around 5 μM, much higher than the reported free solution value but similar to that obtained when one of the binding partners is immobilized on the surface.[6,19–21] This variation might be attributed to the restriction in degree of freedom for the movement of SA or limited access to the binding sites on SA after immobilization.[21]

The sensorgram for the lowest biotin concentration (10 nM) is shown in Fig. 4(c). This concentration is much lower than that used in many other label-free optical biosensors.[15–19] It can be clearly seen that the biotin binding results in a 0.23 pm shift after 800 s, corresponding to a surface mass density of 1.6 pg/mm^2. The standard deviation, δ, is 0.0203 pm, leading to a surface mass density NEDL of 0.14 pg/mm^2, which breaks the 1 pg/mm^2 barrier for many label-free optical biosensors. Finally, control experiments are carried out in Fig. 4(d) by pumping 1 mM biotin through the OFRR immobilized with bovine serum albumin (BSA). After rinse, the sensing signal shows nearly no specific binding between biotin and BSA.

In summary, we have experimentally demonstrated the excellent sensing capability of the ring resonator as a label-free optical biosensor. 2.8×10^{-7} RIU change in bulk RI detection and 1.6 pg/mm^2 of surface mass density detection have been observed. The NEDL is 3.8×10^{-8} RIU and 0.14 pg/mm^2, respectively, which breaks the barrier of 10^{-7} RIU and 1 pg/mm^2 typically encountered in many label-free optical biosensors. The results presented here, along with single particle detection capability recently demonstrated,[4,22] make the ring resonator a highly competitive sensing technology platform.

This work is supported by the Wallace H. Coulter Foundation Early Career Award. H.L. is supported by China Scholarship Council (No. 2009610120) and by the University of Michigan.

[1] X. Fan, I. M. White, S. I. Shopova, H. Zhu, J. D. Suter, and Y. Sun, Anal. Chim. Acta **620**, 8 (2008).
[2] F. Vollmer, D. Braun, A. Libchaber, M. Khoshsima, I. Teraoka, and S. Arnold, Appl. Phys. Lett. **80**, 4057 (2002).
[3] H. Zhu, I. M. White, J. D. Suter, P. S. Dale, and X. Fan, Opt. Express **15**, 9139 (2007).
[4] F. Vollmer, S. Arnold, and D. Keng, Proc. Natl. Acad. Sci. U.S.A. **105**, 20701 (2008).
[5] H. Zhu, P. S. Dale, C. W. Caldwell, and X. Fan, Anal. Chem. **81**, 9858 (2009).
[6] M. Iqbal, M. A. Gleeson, B. Spaugh, F. Tybor, W. G. Gunn, M. Hochberg, T. Baehr-Jones, R. C. Bailey, and L. C. Gunn, IEEE J. Sel. Top. Quantum Electron. **16**, 654 (2010).
[7] Y. Sun and X. Fan, Opt. Express **16**, 10254 (2008).
[8] S. Arnold, M. Khoshsima, I. Teraoka, S. Holler, and F. Vollmer, Opt. Lett. **28**, 272 (2003).
[9] I. M. White and X. Fan, Opt. Express **16**, 1020 (2008).
[10] I. M. White, H. Oveys, and X. Fan, Opt. Lett. **31**, 1319 (2006).
[11] T. Ling and L. J. Guo, Opt. Express **15**, 17424 (2007).
[12] X. Fan, I. M. White, H. Zhu, J. D. Suter, and H. Oveys, Proc. SPIE **6452**, 64520M (2007).
[13] L. Kou, D. Labrie, and P. Chylek, Appl. Opt. **32**, 3531 (1993).
[14] D. Markov, D. Begari, and D. J. Bornhop, Anal. Chem. **74**, 5438 (2002).
[15] B. Lin, J. Qiu, J. Gerstenmeier, P. Li, H. M. Pien, J. Pepper, and B. Cunningham, Biosens. Bioelectron. **17**, 827 (2002).
[16] K. Cottier, M. Wiki, G. Voirin, H. Gao, and R. E. Kunz, Sens. Actuators B **91**, 241 (2003).
[17] M. J. Swann, L. L. Peel, S. Carrington, and N. J. Freeman, Anal. Biochem. **329**, 190 (2004).
[18] A. V. Kabashin, P. Evans, S. Pastkovsky, W. Hendren, G. A. Wurtz, R. Atkinson, R. Pollard, V. A. Podolskiy, and A. V. Zayats, Nature Mater. **8**, 867 (2009).
[19] Y. Guo, J. Y. Ye, C. Divin, B. Huang, T. P. Thomas, J. J. R. Baker, and T. B. Norris, Anal. Chem. **82**, 5211 (2010).
[20] Y. J. Tang, R. Mernaugh, and X. Q. Zeng, Anal. Chem. **78**, 1841 (2006).
[21] T. Arai, P. K. R. Kumar, C. Rockstuhl, K. Awazu, and J. Tominaga, J. Opt. A, Pure Appl. Opt. **9**, 699 (2007).
[22] J. G. Zhu, S. K. Ozdemir, Y. F. Xiao, L. Li, L. N. He, D. R. Chen, and L. Yang, Nat. Photonics **4**, 46 (2010).